Optics Letters

Folded thin-film lithium niobate modulator based on a poled Mach–Zehnder interferometer structure

JINYAO HU,[1] CHIJUN LI,[1] CHANGJIAN GUO,[1,2] CHAO LU,[2] ALAN PAK TAO LAU,[3]
PENGXIN CHEN,[1,5] AND LIU LIU[4,*]

[1] Centre for Optical & Electromagnetic Research, Guangdong Provincial Key Laboratory of Optical Information Materials and Technology, South China Academy of Advanced Optoelectronics, Sci. Bldg. No. 5, South China Normal University, Higher-Education Mega-Center, Guangzhou 510006, China
[2] Photonics Research Center, Department of Electronic and Information Engineering, The Hong Kong Polytechnic University, Hong Kong SAR, China
[3] Photonics Research Center, Department of Electrical Engineering, The Hong Kong Polytechnic University, Hong Kong SAR, China
[4] State Key Laboratory for Modern Optical Instrumentation, Centre for Optical & Electromagnetic Research, College of Optical Science and Engineering, International Research Center for Advanced Photonics, Zhejiang University, East Building No. 5, Zijingang Campus, Hangzhou 310058, China
[5] e-mail: chenpx@m.scnu.edu.cn
*Corresponding author: liuliuopt@zju.edu.cn

Received 30 March 2021; revised 12 May 2021; accepted 13 May 2021; posted 17 May 2021 (Doc. ID 426083); published 14 June 2021

The thin-film lithium niobate structure has been used recently to construct compact and high-performance electro-optical modulators. Due to the moderate electro-optical coefficient of the lithium niobate material, the device length of such a modulator is still long, a few centimeters usually. Here, a folded Mach–Zehnder interferometer based modulator on *x*-cut thin-film lithium niobate is demonstrated. An effective poling procedure is developed to activate the device. The proposed modulator structure can shorten the device length without affecting its performance. The measured $V_\pi L$ product of a fabricated and completely poled folded modulator is about 2.74 V · cm, and the 3 dB electro-optical bandwidth is about 55 GHz. They are close to those of a conventional Mach–Zehnder modulator with a straight modulation section.

https://doi.org/10.1364/OL.426083

The electro-optical (EO) modulator is one of the key functional devices in optical fiber communication systems [1], with which the driving electrical signal can be converted on an optical carrier, and transmits in the optical domain [2]. Lithium niobate (LN) has excellent physical properties, such as a wide transparent bandwidth, strong EO coefficient, good thermal stability, etc., and is widely considered as the ideal material to fabricate high-performance EO modulators [3–9]. Normally, EO modulators based on LN can be implemented in a variety of forms, e.g., a Mach–Zehnder interferometer (MZI) [6–9], microresonator [3], photonic crystals [10], etc. Among them, the MZI based modulator on *x*-cut LN material has a large working wavelength range, and naturally supports chirp-free operation and a push–pull configuration (which reduces the modulation voltage by a factor of two) [11]. These advantages render it one of the main modulator forms on LN. Traditional bulk LN EO modulators are usually fabricated by proton exchange or ion diffusion. They typically have a large optical mode size with weak light confinement due to the low index contrast (<0.02) between the core and cladding, which further results in a large bend radius [1–4]. Therefore, it is not suitable for highly integrated circuits. In recent years, the thin-film LN-on-insulator (LNOI) has shown great potential to overcome these disadvantages. It provides a high index contrast using low refractive index materials, e.g., air or silicon dioxide, as the cladding layer [6–9]. Therefore, the driving voltage of such a modulator has been largely decreased due to the reduced mode size. Nevertheless, the length of a MZI modulator built on LNOI is still long due to the moderate EO coefficient of the LN material. The typical length is about a few millimeters, or even more than 2 cm to obtain a low modulation voltage directly driven with CMOS circuitry [3]. On the other hand, the width of MZIs is just about a few hundred micrometers including the electrodes. The slender structure imposes difficulties in integration with other devices in a large-scale circuit, as well as packaging. In addition, the long modulation section may also exceed the reticle size of a lithography tool for some applications.

One straightforward approach to reduce the device length of such a modulator is to fold the arms of the MZI, as shown in Fig. 1 (one arm is shown). However, due to the presence of the 180° turn, the direction of the applied electric field changes also after the turn, as shown in Fig. 1(a). For *x*-cut LN, the optical axis *z* remains the same across the whole wafer. This will cancel out the phase change accumulation for modulation in this arm. In this Letter, we demonstrate a solution to this problem by using a poled and folded MZI (FMZI) structure. The poling process can invert the local crystal domain of LN [12], which

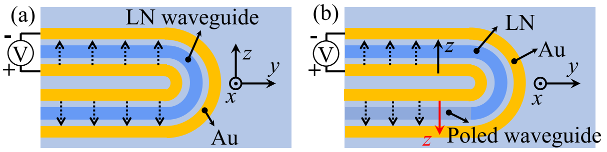

Fig. 1. Relation of the z axis of the LN material and direction of the applied electric field on one arm of the MZI (a) before poling and (b) after poling.

can then keep the direction of the LN $+z$ axis aligned to the applied electric field before and after the turn, as shown in Fig. 1(b). The LN material can be poled using, e.g., scanning-probe microscopy [13] or strong electric field [12]. The latter one is adopted in this Letter.

The three-dimensional (3D) structure of the proposed FMZI modulator using the push–pull configuration is shown in Fig. 2(a). The modulator is fabricated on a commercial x-cut LNOI wafer (NanoLN, Jinan, China) with 400 nm thick LN film. The LN waveguide has a ridge height of 200 nm, i.e., half the thickness of the LN film. Between the thin film LN and the silicon substrate, a 3 μm thick thermal oxide is present. A multimode interferometer (MMI) made on LN, which has a relaxed fabrication tolerance and a large wavelength bandwidth [14], is used as the 3 dB splitter and combiner for the MZI [14]. Grating couplers (GCs) using amorphous silicon stripes [15] are used as fiber-to-chip interfaces. Traveling wave (TW) electrodes based on a classic coplanar waveguide (CPW), in which electric and optical waves propagate collinearly, is also adopted in the proposed MZI. It supports a quasi-transverse electromagnetic (quasi-TEM) mode for the electrical signal with low dispersion, and therefore can offer a high modulation bandwidth [11].

Since the characteristics of an MZI modulator are mainly determined by the cross section of the modulation section, which is labeled and shown in Figs. 2(a) and 2(b), the structural parameters of this cross section are optimized first using a multi-physics model based on a finite element algorithm [1,4,16]. Au is used here as the electrode material, considering its good conductivity and stability. Its thickness is 1.1 μm, which is at a good balance between performance and cost [17]. The top width of the LN ridge waveguide in the modulation section is 4.0 μm, which is also optimal considering the modulation bandwidth [17]. A wider waveguide also facilitates the fabrication process, since ultraviolate (UV) contact photolithography was employed to define the LN pattern. The width of the routing waveguide is 1.5 μm to suppress the high-order mode excitation. The gap between the electrode and the LN waveguide has a major effect on the product ($V_\pi L$) of the half-wave voltage (V_π) and the length (L) of the modulator [1,17]. A relatively large gap of 2.0 μm between the electrode and the LN waveguide is used here, taking into account the precision of the lithography alignment and the balance between the $V_\pi L$ product and the optical loss. The width of the signal electrode is 14 μm. The RF loss α_m, RF effective refractive n_m, and the characteristic impedance Z_0 obtained from the simulation are shown in Figs. 2(c)–2(e), respectively. The index matching between the RF and optical modes and the impedance matching between the CPW and the source/load (50Ω) are not perfect in this design. The simulated $V_\pi L$ product is 3.0 V · cm.

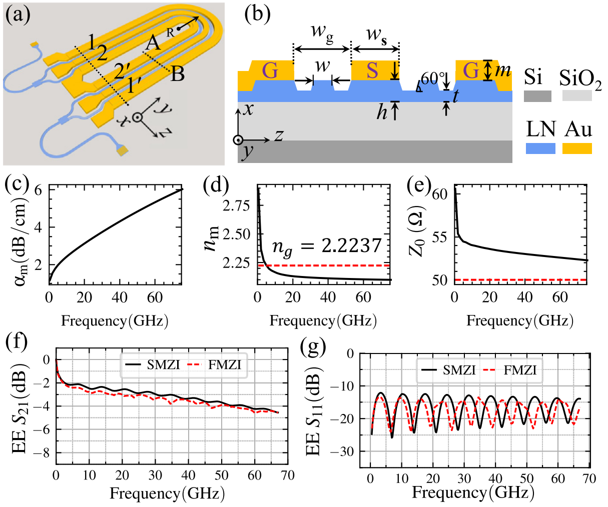

Fig. 2. (a) 3D structure of the proposed FMZI modulator. (b) Cross section of the modulation section labeled as AB in (a). G, ground electrode; S, signal electrode. Structural parameters: $t = 200$ nm, $h = 400$ nm, $w = 4.0$ μm, $w_g = 8.0$ μm, $w_s = 14$ μm, $m = 1.1$ μm. Simulation results of (c) RF loss, (d) RF effective index n_m, and (e) characteristic impedance Z_0. In (d), the red-dashed line is the optical group index n_g. In (e), the red-dashed line is 50Ω. Simulated EE (f) S_{11} and (g) S_{21} responses of the SMZI and FMZI modulators.

For a proper 180° turn in the proposed FMZI structure, both electrical and optical modes should be considered. Due to the high index contrast provided by LNOI, the bend radius for a LNOI waveguide can be as small as 5 μm [18]. However, a too small bend would easily induce polarization coupling due to the anisotropy of LN [19]. The quasi-TEM mode of the CPW will also exhibit a strong reflection due to the mode mismatch at the interface between the bend and straight electrodes. Our simulations and measurements of fabricated CPWs suggest that the bend radius of the CPW should be larger than 50 μm to suppress the reflection. In the proposed FMZI, the radius of the bend is 100 μm measured from the center of the signal electrode, as shown in Fig. 2(a), and the radii of the two LN waveguides are 89 μm and 111 μm. The length of the straight modulation section is 5.0 mm, and therefore, effectively the total modulation section is 1 cm long in the present FMZI. Although some residual modulation could exist in the bending section, it is expected to be small due to the short length (compared to the total modulation length) and the misaligned optical axis to the electrical field. Finally, the 3D model of the designed FMZI is simulated, and the electro-electrical (EE) frequency responses are plotted in Figs. 2(f) and 2(g). As a comparison, a straight MZI (SMZI) structure with the same crossing section parameters and total modulation length is also simulated. The S_{11} responses of the FMZI and SMZI are relatively high and show Fabry–Perot characteristics, which are mainly induced by the impedance mismatch. The EE S_{21} response of FMZI is slightly worse than that of SMZI, which is due to the extra CPW length from the bend. Note that the modulator performance can be further optimized following the procedure discussed in Ref. [17].

The designed FMZI modulator was then fabricated. First, the LN waveguides were patterned and etched using UV contact lithography and inductively coupled plasma reactive ion etching. Then, another patterning and a lift-off process were used to fabricate TW electrodes. After that, amorphous silicon GCs were prepared using e-beam lithography and lift-off as

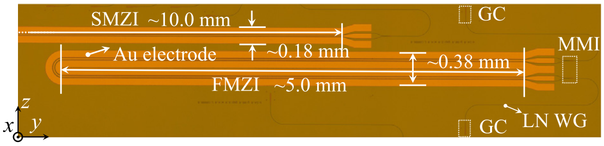

Fig. 3. Microscope picture of the fabricated MZI modulators.

well [15]. The measured coupling loss of the fabricated GC is about −18 dB due to the loss of the fabricated amorphous silicon. The GC can be optimized using Au gratings, as discussed in Ref. [20]. Optical insertion losses of the SMZI and the FMZI are about −7.5 dB and −8.5 dB, respectively. Simulations and separate experiments show that the 180° bend of the LN waveguide used here should exhibit negligible losses [19]. The extra 1 dB loss for the FMZI in the present sample probably results from fabrication variations. A microscope picture of the fabricated FMZI modulator is presented in Fig. 3. A reference SMZI is also fabricated, which is shown in part. The lengths of the modulation sections in the SMZI and FMZI are the same, i.e., 1 cm. Due to the folding, the device length of the FMZI is almost half that of the SMZI.

As mentioned above, a poling process is necessary to activate the FMZI modulator. Here, the CPW electrodes can be used directly as the poling electrodes without any additional fabrication steps. The poling process is shown in Fig. 4 in detail. The cross section of the modulation section, labeled as 122′1′ in Fig. 2(a), is shown in Fig. 4(a), as well as the electrical field distributions when the signal electrode is driven. In this case, the EO effect is cancelled in both arms of the FMZI. The whole poling process consists of two steps. First, a high voltage (HV) was applied in the arm of waveguide 1 and waveguide 1′, as shown in Fig. 4(b). To prevent an unwanted poling effect in the other arm, the two electrodes beside the arm of waveguide 2 and waveguide 2′ were tied together. One can find that in this poling process, the local LN domain only in waveguide 1 will be reversed by the applied HV. Second, a similar procedure was used to pole the other arm of the FMZI, as shown in Fig. 4(c), where the local domain of waveguide 2 is reversed. To avoid the electrode breakdown caused by arcing, the device was covered with silicone oil during poling [12]. Unlike the case in fabricating a periodically poled LN structure, where the waveform of HV pulses needs to be fine-tuned to control the duty cycle of the poling result [12], the poled area here is large, and it holds no danger of over-poling. The HV pulses used here were square pulses with 100–300 V (set values of the HV source) peak-to-peak amplitude (V_{pp}), 5 Hz frequency, and 30% duty cycle, and the total poling duration for each step was about 10 s.

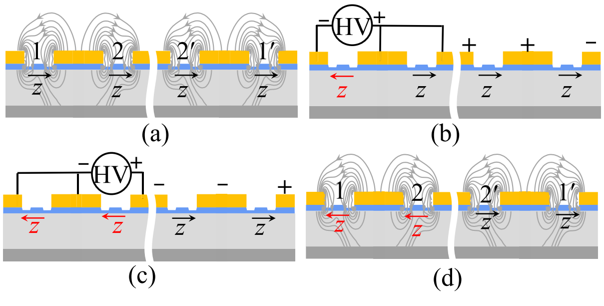

Fig. 4. (a) Electrical field and z axis of the LN before poling. (b) First step and (c) second step of the poling process. (d) Electrical field and z axis of LN after poling.

Other forms of pulses may also be applicable as long as they are strong and long enough. After the above poling process, the axis of the LN material and the electrical field during modulation would be aligned along each whole arm of the FMZI, as shown in Fig. 4(d).

For characterization, first the V_π of the fabricated FMZI modulator were measured using 500 kHz triangular waves each time after one poling process, where the poling V_{pp} increased from 100 V to 300 V. When the poling V_{pp} are less than 100 V, the FMZI could not work. From 150 V poling, as shown in Fig. 5(a), the FMZI starts to show modulation responses. Yet, the modulation is still not strong enough to cover a whole MZI response for the voltage sweep here. Therefore, a fitting using a sinusoidal function was applied to extract the V_π. Until the poling V_{pp} increases to 225 V, a whole MZI response can be measured, as shown in Fig. 5(a) as well. The measured or fitted $V_\pi L$ at different poling V_{pp} is plotted in Fig. 5(b). One can find that the $V_\pi L$ products decrease as the poling voltage increases. For reference, the $V_\pi L$ product of the SMZI fabricated on the same chip was also measured, which is $2.6\ \mathrm{V \cdot cm}$ close to the simulation. When the poling V_{pp} reached 300 V for the FMZI, a complete poling for the desired area happened, i.e., the $V_\pi L$ products of the FMZI ($2.74\ \mathrm{V \cdot cm}$) and SMZI are almost the same. The poling electrical field in this case is about $27\ \mathrm{kV\ mm^{-1}}$, which is close to the previously reported value for poling undoped LN [21].

The small signal EO bandwidth of the FMZI and SMZI modulators were then characterized using a vector network analyzer. A tunable laser was used as the optical source, and the modulated light was collected by a photodiode of 70 GHz bandwidth. A RF probe was used to deliver the electrical signal to the pads of the modulator. The CPW was terminated with a 50Ω resistor. The EO response of the fabricated MZI modulators are

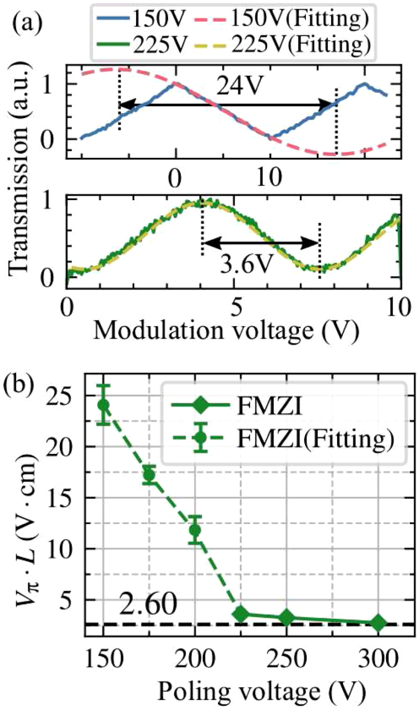

Fig. 5. (a) Normalized optical transmissions as a function of applied modulation voltages for 150 V and 225 V poling. (b) Measured $V_\pi L$ products as a function of poling voltages. The measured $V_\pi L$ of the reference SMZI is also plotted in (b) with a dashed line.

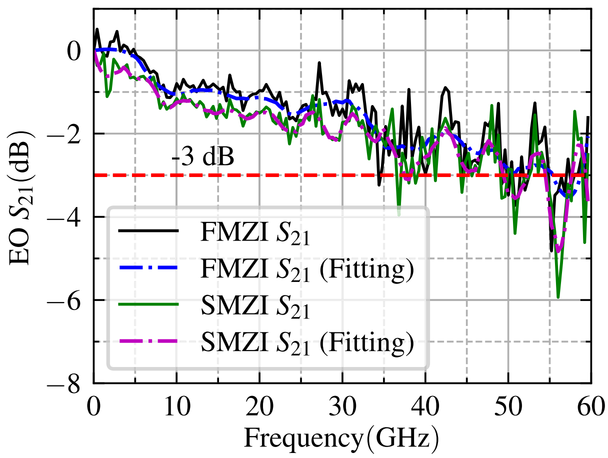

Fig. 6. EO responses of the fabricated FMZI and SMZI modulators.

shown in Fig. 6, where the responses of the RF cables, the RF probes, and the photodetector are calibrated out. The curves are noisy due to the high losses of the GCs. Nevertheless, the measured 3 dB EO bandwidths of the FMZI and SMZI modulators are both about 55 GHz, which implies that the poling process here works as desired and would not affect the performance of the modulator. In principle, for a TW modulator with a perfect index and impedance matching, the 3 dB EO bandwidth would be the same as the 6.4 dB EE bandwidth [22], which is over 70 GHz as shown in Fig. 2(f) for simulations. In the present structure, there still exists unmatching in the index and the impedance as mentioned before. Therefore, the measured EO bandwidth is slightly less.

In this Letter, we have demonstrated an FMZI modulator on an x-cut LNOI wafer using a poling technique. The device length can then be made twice as short. The basic device structures here are the same as those of common modulators on LNOI, and need no additional fabrication steps, except for poling. A two-step poling process has been developed to activate the folded modulator. The measured modulation strength of the fabricated FMZI modulator under different poling voltages implies that if complete poling is achieved, the $V_\pi L$ product can be close to that of the common SMZI modulator with the same structural parameters and modulation length. The measured EO response further indicates that the poling process would not deteriorate the modulation performance of the modulator. In the present demonstration, only one 180° turn was employed in the FMZI. Nevertheless, the same device principle and poling process can be applied for more turns, where the device length of an FMZI can be further decreased in expense of its width.

Funding. National Key Research and Development Program of China (2019YFB1803902); Science and Technology Planning Project of Guangdong Province (2019A050510039); Natural Science Foundation of Guangdong Province (2018A0303130117); Fundamental Research Funds for the Central Universities (2021QNA5001).

Acknowledgment. The authors thank Hongying Chen and Prof. Xingsen Gao for their assistance on poling and useful discussions.

Disclosures. The authors declare no conflicts of interest.

Data Availability. Data underlying the results presented in this paper are not publicly available at this time but may be obtained from the authors upon reasonable request.

REFERENCES

1. A. Honardoost, F. A. Juneghani, R. Safian, and S. Fathpour, Opt. Express **27**, 6495 (2019).
2. P. O. Weigel, F. Valdez, J. Zhao, H. Li, and S. Mookherjea, J. Phys. Photon. **3**, 012001 (2020).
3. C. Wang, M. Zhang, B. Stern, M. Lipson, and M. Lončar, Opt. Express **26**, 1547 (2018).
4. A. Honardoost, R. Safian, A. Rao, and S. Fathpour, J. Lightwave Technol. **36**, 5893 (2018).
5. T. Ren, M. Zhang, C. Wang, L. Shao, C. Reimer, Y. Zhang, O. King, R. Esman, T. Cullen, and M. Lončar, IEEE Photon. Technol. Lett. **31**, 889 (2019).
6. M. Xu, M. He, H. Zhang, J. Jian, Y. Pan, X. Liu, L. Chen, X. Meng, H. Chen, Z. Li, X. Xiao, S. Yu, S. Yu, and X. Cai, Nat. Commun. **11**, 3911 (2020).
7. P. Ying, H. Tan, J. Zhang, M. He, M. Xu, X. Liu, R. Ge, Y. Zhu, C. Liu, and X. Cai, Opt. Lett. **46**, 1478 (2021).
8. M. He, M. Xu, Y. Ren, J. Jian, Z. Ruan, Y. Xu, S. Gao, S. Sun, X. Wen, L. Zhou, L. Liu, C. Guo, H. Chen, S. Yu, L. Liu, and X. Cai, Nat. Photonics **13**, 359 (2019).
9. S. Sun, M. He, M. Xu, S. Gao, Z. Chen, X. Zhang, Z. Ruan, X. Wu, L. Zhou, L. Liu, C. Lu, C. Guo, L. Liu, S. Yu, and X. Cai, Photon. Res. **8**, 1958 (2020).
10. M. Li, J. Ling, Y. He, U. A. Javid, S. Xue, and Q. Lin, Nat. Commun. **11**, 4123 (2020).
11. E. L. Wooten, K. M. Kissa, A. Yi-Yan, E. J. Murphy, D. A. Lafaw, P. F. Hallemeier, D. Maack, D. V. Attanasio, D. J. Fritz, G. J. McBrien, and D. E. Bossi, IEEE J. Sel. Top. Quantum Electron. **6**, 69 (2000).
12. Y. Jiao, Z. Shao, S. Li, X. Wang, F. Bo, J. Xu, and G. Zhang, Materials **13**, 3617 (2020).
13. J. Nagy and R. Reano, Opt. Mater. Express **9**, 3146 (2019).
14. L. B. Soldano and E. C. M. Pennings, J. Lightwave Technol. **13**, 615 (1995).
15. Z. Chen, Y. Wang, H. Zhang, and H. Hu, Opt. Mater. Express **8**, 1253 (2018).
16. A. Chowdhury and L. McCaughan, Opt. Lett. **26**, 1317 (2001).
17. J. Cai, C. Guo, C. Lu, A. P. T. Lau, P. Chen, and L. Liu, "Design optimization of silicon and lithium niobate hybrid integrated traveling-wave Mach–Zehnder modulator," IEEE Photon. J. (to be published).
18. A. Rao and S. Fathpour, IEEE J. Sel. Top. Quantum Electron. **24**, 3400114 (2018).
19. J. Wang, P. Chen, D. Dai, and L. Liu, IEEE Photon. J. **12**, 2200310 (2020).
20. Z. Ruan, J. Hu, Y. Xue, J. Liu, B. Chen, J. Wang, K. Chen, P. Chen, and L. Liu, Opt. Express **28**, 35615 (2020).
21. H. Zhang, H. Zhu, Q. Li, and H. Hu, Opt. Mater. **109**, 110364 (2020).
22. M. Xu, W. Chen, M. He, X. Wen, Z. Ruan, J. Xu, L. Chen, L. Liu, S. Yu, and X. Cai, APL Photon. **4**, 100802 (2019).